Wear 368-369 (2016) 368–378

Contents lists available at ScienceDirect

Wear

journal homepage: www.elsevier.com/locate/wear

Effect of alternate corrosion and wear on the overall degradation of a dual phase and a mild steel

Pratik Murkute [a], J. Ramkumar [b], S. Choudhary [c], K. Mondal [c,*]

[a] Materials Science Programme, Indian Institute of Technology Kanpur, Uttar Pradesh, India
[b] Department of Mechanical Engineering, Indian Institute of Technology Kanpur, Uttar Pradesh 208016, India
[c] Department of Materials Science and Engineering, Indian Institute of Technology Kanpur, Uttar Pradesh 208016, India

ARTICLE INFO

Article history:
Received 28 May 2016
Received in revised form
26 September 2016
Accepted 29 September 2016
Available online 1 October 2016

Keywords:
Sliding wear
Steel, Corrosion-wear
Immersion corrosion
Surface analysis

ABSTRACT

The present work investigates the alternate corrosion and wear effect on the overall degradation of a dual phase and a mild steel. In case of corrosion-wear, immersion corroded samples of both the steels in freely aerated 3.5 wt% NaCl solution are subjected to reciprocating sliding wear at three different loads. In case of wear-corrosion, wear takes place first in the steel samples, which are then subjected to immersion corrosion. The wear volume and mean coefficient of friction have decreased for the corrosion-wear case as compared to only wear, and this attributes to the lubricating action of rust formed due to initial corrosion. In case of wear-corrosion, corrosion rates of both the samples have increased as compared to only corrosion situation, which attributes to the rough and strained surface created due to initial wear. Though both the trends are independent of types of steels, the overall wear of the dual phase steel is lower than that of the mild steel, whereas, corrosion rate of the dual phase steel is higher than the mild steel in both the corrosion-wear and wear-corrosion cases.

1. Introduction

Dual phase steel (DPS) and mild steel (MS) are the two major varieties of steel in a large pool of different types of steels, which are extensively used in various structural applications. DPS, from structural and engineering viewpoint, gives a very good combination of strength and toughness together due to its unique structure consisting of martensite islands in a matrix of polygonal ferrite. The DPS has higher hardness and is supposed to have superior wear resistance as compared to MS because MS consists of small fraction of pearlite in a matrix of polygonal ferrite [1]. The grain size of process annealed MS is higher than that of the intercritically annealed DPS, resulting finer grain size in the DPS. This fine grain microstructure of the DPS also leads to higher abrasion or wear resistance as compared to the MS [1].

Tribological properties of DPS and MS have been extensively studied by the researchers [2–9]. Extensive literature is available on the effect of morphology and volume fraction of martensite on the tensile and tribological properties of DPS. Bayram and Uguz [9] have studied the effect of microstructure on the wear behavior of DPS and found that increased ductility leads to increased wear in DPS. Xu et al. [5,10] have observed that under high load conditions, for all the DPS morphologies, scratch resistance is only affected by the martensite fraction. Fine granular martensite islands have the best low-hardness abrasion resistant steel for mild abrasion conditions, while for aggressive work conditions, DPS with fine (granular or fibrous) martensite structures have best abrasion resistance. Ahmad et al. [11] have concluded that specimen with bulk morphology of high carbon martensite particles has minimum plastic deformation in comparison to grain boundary connected, scattered laths morphologies of the martensite.

Exhaustive research works on tribological behavior of plain carbon steel have already been carried out [3,4,8,12–17]. Goto and Amamoto [18] have investigated the effect of varying load on the wear resistance of carbon steel in unlubricated condition. They have discussed the formation of severely oxidized and high hardness work-hardened surface at higher sliding loads, resulting in quasi-mild wear mode, which has very high endurance. This quasi-mild wear mode protects the steel surface from severe wear damage and it extends upto very high loads. They have also talked about the improvement of wear resistance for carbon steel under unlubricated sliding and variable loading conditions by the similar quasi-mild wear mode formation [12]. Islam et al. [19] have investigated the effect of microstructure on the erosion behavior of carbon steel, and observed that pearlite phase with lamellar structure has higher erosion resistance than ferrite phase.

The corrosion behavior of DPS and MS is a function of microstructure, grain size and also their chemical composition.

* Corresponding author.
E-mail address: kallol@iitk.ac.in (K. Mondal).

http://dx.doi.org/10.1016/j.wear.2016.09.027
0043-1648/

Table 1
Composition of the dual phase steel and the mild steel along with hardness and yield strength values.

	%C	%Mn	%Si	%Cr	% Cu	%Co	%Mo	%Ni	%Al	% P	% S
DPS	0.20	0.70	0.25	0.01	0.01	0.01	0.01	0.01	0.04	0.03	0.03
MS	0.02	0.71	0.24	0.01	0.01	0.01	0.01	0.01	0.03	0.01	0.01
Hardness value (VHN)				DPS: 240–250			MS: 130–135			Steel Ball: 800–900	
Yield strength (MPa)				DPS: 330				MS: 250			

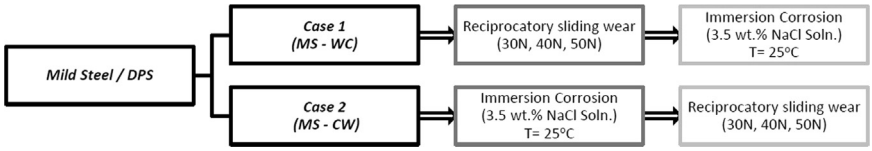

Fig. 1. Schematic of sequence of testing followed during the study (WC: Wear-Corrosion CW: Corrosion-Wear).

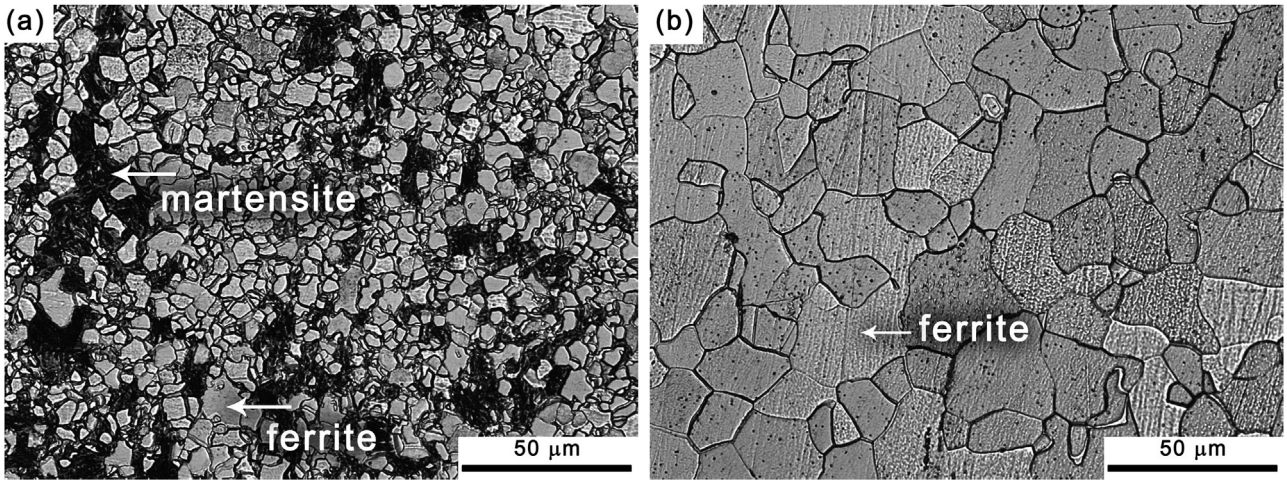

Fig. 2. Optical micrographs of the (a) dual phase steel (b) mild steel.

Intercritically annealed DPS, which has a finer grain size as compared to a process annealed coarse grained MS, has higher uniform corrosion rate in both acidic and neutral electrolytic medium [20] during immersion. The effect of microstructure has been studied by Sarkar et al. [21], and they have shown that larger volume fraction and finer martensite morphology decrease the corrosion resistance of the DPS. Bhagavathi et al. [22] have also investigated the corrosion behavior of a plain low carbon steel. Different rust morphologies formed during the exposure of carbon steels to marine atmospheres have been analyzed too [23].

In addition, there are studies on the erosion corrosion behavior of plain carbon steels [4,24–28]. Stack et al. [29] have investigated the erosion–corrosion of chromium steel in a rotating cylinder electrode system in NaOH solution, and found that for slurry erosion–corrosion of low carbon, increase in flow velocity results in higher current densities for the anodic reaction. Generally, increase in flow velocity increases the erosion-corrosion of materials due to impingement effect on the walls of the structure. If the flowing system contains suspended hard particles, it would lead to enhanced wear too. Increase in particle size has resulted in an overall increase in erosion–corrosion rate. Although, above a critical value, the erosion–corrosion rate has been found to be independent of particle size, and similar behavior pertains also to erosion.

Though there are studies on corrosion and wear of steel independently, it is of high relevance if the effect of corrosion-wear or wear-corrosion on the overall degradation of steels is studied. Even, simultaneous effect of wear and corrosion (erosion-corrosion) has been studied. It is quite understood that in many practical applications, where meeting surfaces, such as rails, experience corrosion as well wear in an alternate fashion. Either corrosion happens and then wear takes place, or wear is followed by corrosion. Corrosion and wear do not happen simultaneously in such applications. Therefore, it is important to study the effect of initial wear on the corrosion rate of materials, as well effect of initial corrosion on the wear effect of the material. Finally, alternate corrosion and wear (corrosion-wear or wear-corrosion) would have their effect on the overall degradation of materials. However, such an important aspect has not been studied much. Although exact simulation of the actual conditions is not possible at a laboratory scale, we have employed 3.5 wt% NaCl solution as a working electrolyte since this is widely studied reference condition. This also mimics the highly corrosive marine environment.

Therefore, the present study aims at finding the effect of corrosion-wear as well wear-corrosion on the degradation of two steels, a DPS and a MS, when corrosion and wear happen alternatively. Therefore, experiments have been designed such a fashion that in case of corrosion-wear, immersion corrosion takes place first and the corroded sample is subjected to reciprocating sliding wear. In another set (wear-corrosion), the reciprocating sliding wear takes place first, and then the worn sample is subjected to immersion test. The present work also tries to understand the mechanisms of different behavior shown by two different steels subjected to corrosion-wear and wear-corrosion.

2. Material and methods

The composition, hardness and yield strength of a DPS and a

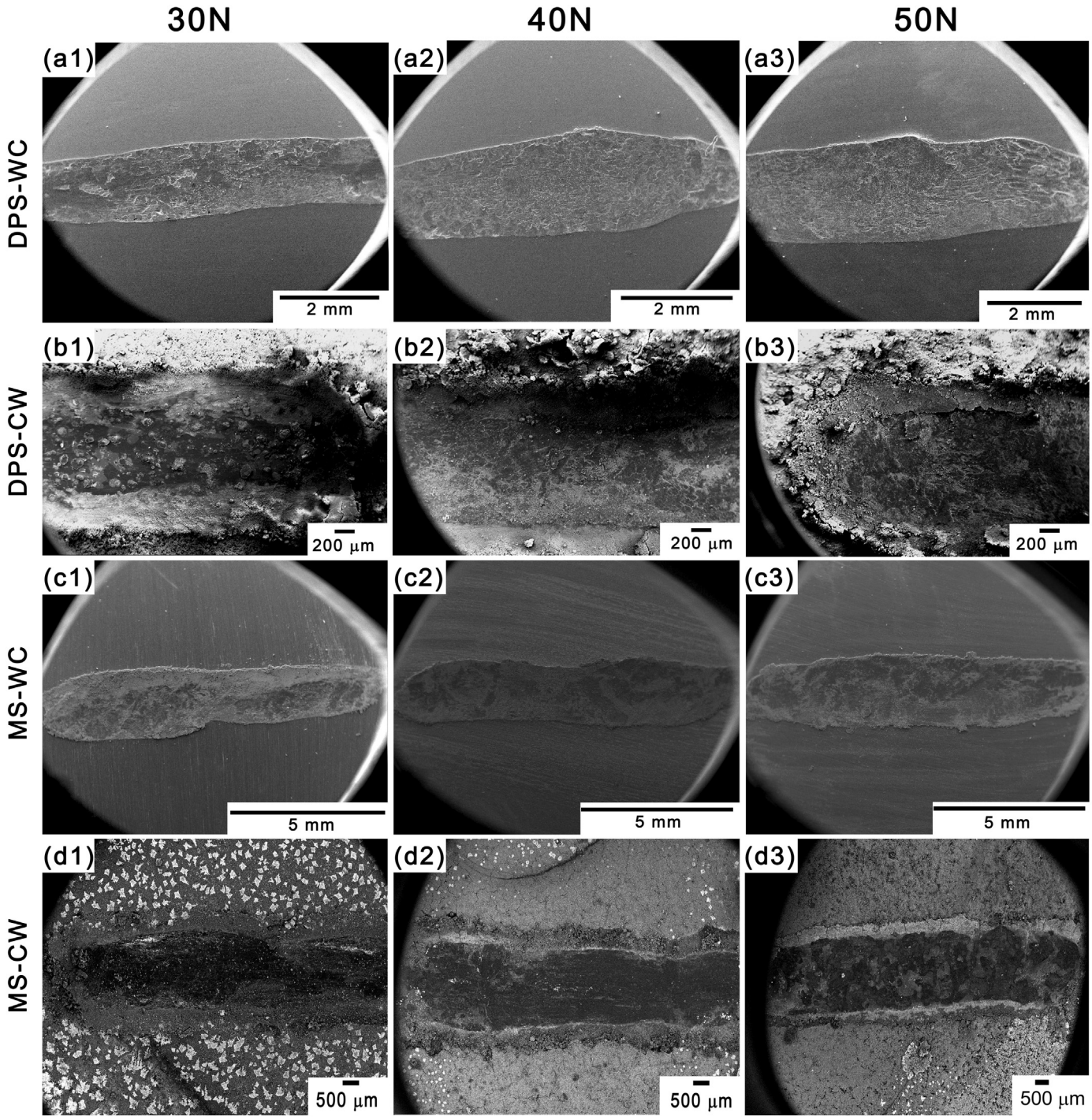

Fig. 3. Wear scar morphologies at various loads in (a1–a3) DPS-WC (b1–b3) DPS-CW (c1–c3) MS-WC (d1–d3) MS-CW.

MS used in this study are given in Table 1. Cuboid specimens of 20 mm × 20 mm × 5 mm were mechanically ground to grit size 2500 of emery paper, followed by cloth polishing using alumina paste of 5 and 1 μm to obtain a mirror finish sample. Ultrasonic cleaning was done in acetone for 10 min to ensure complete removal of alumina particles. Then the dried steel samples were weighed using a microbalance. For microstructural analysis, the samples were etched with 2% Nital solution. Microstructures of the DPS and MS samples were observed using Leica 6000 M optical microscope. The experimentation sequence is shown in Fig. 1.

In the Case 1 (WC), samples of the DPS and the MS were subjected to wear test on the polished steel surface initially, and then the worn samples without disturbing and doing further processing) were subjected to immersion corrosion. For immersion corrosion tests, the corrosive medium used was freely aerated 3.5 wt% NaCl solution. The exposure period of all the immersion tests was 10 days. All the samples were hung parallel to the ground i.e. at an angle of 0° to the ground. Only skyward face of the samples was exposed to the NaCl solution, while rest of the faces was covered with anticorrosion lacquer and teflon tape. Weight of the steel specimen was noted before and after immersion corrosion test to quantify the corrosion rate via weight loss method post immersion corrosion. For the Case 2 (CW), the DPS and the MS samples were subjected to immersion corrosion tests initially, and then wear

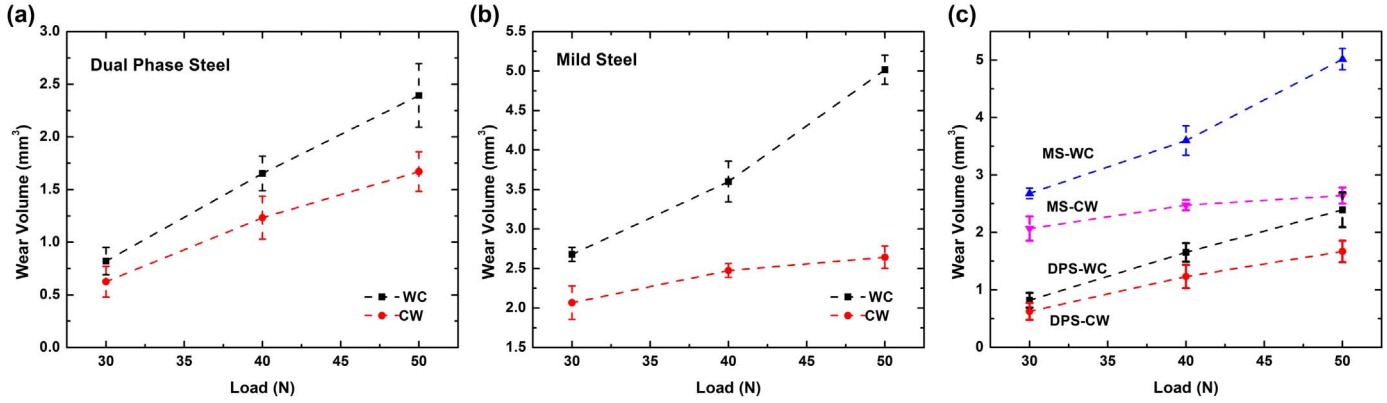

Fig. 4. Wear volumes at various loads for the (a) DPS and (b) MS for WC and CW cases. (c) Comparison of wear volume of the DPS and MS.

Table 2
Hertzian contact pressure, wear volume and mean C.O.F at various normal loads. The corrosion rate of the DPS and MS in case of the CW case are same at all three loads.

Load			30 N	40 N	50 N
Hertzian contact pressure (MPa)			1.65 GPa	1.82 GPa	1.96 GPa
Wear volume (mm^3)	DPS	WC	0.82	1.65	2.39
		CW	0.63	1.23	1.67
	MS	WC	2.68	3.60	5.02
		CW	2.07	2.48	2.64
Mean C.O.F	DPS	WC	0.15	0.26	0.33
		CW	0.08	0.14	0.17
	MS	WC	0.19	0.22	0.23
		CW	0.15	0.18	0.19
Corrosion rate (mpy)	DPS	WC	40	44	50
		CW	17		
	MS	WC	30	33	33
		CW	10		

tests were conducted on the corroded surface without disturbing the corroded layer. All the tests were done three times to confirm the repeatability and reproducibility of the results. Wear parameters, like coefficient of friction (C.O.F), wear volume, and wear surface damage, were qualitatively and quantitatively analyzed. Nomenclature used for wear-corrosion is WC (step 1: wear test and step 2: immersion corrosion), and corrosion-wear is CW (step1: immersion corrosion and step 2: wear test).

Post immersion corrosion and wear tests (in WC and CW case), the samples were gently taken out of the solution in order to keep the corrosion products intact and were dried off for about 6 h. Rust morphology was studied using FEI Quanta scanning electron microscope. Rust was then scraped off gently from the dried steel samples. After mechanical removal of rust from the corroded steel samples, the samples were chemically cleaned using Clarke's solution per ASTM G1-03(2011) specification. Post chemical cleaning, the steel samples were again weighed to measure the weight loss and to calculate the corrosion rate. Phase analysis of the powdered rust was performed using X-Ray diffraction (XRD) technique and Fourier transform infrared technique (FTIR). XRD was carried out in a Panalytical diffractometer operated at 40 kV and 30 mA with scanning rate of 0.02/min and Cu-Kα radiation ($\lambda = 1.5406$ A°). The diffracting angle (2θ) ranged from 10 to 100°. Perkin-Elmer Spectrum-2 setup was used for FTIR analysis and the range of wave number scanning was from 450 to 4000 cm^{-1}.

The samples for wear testing were prepared after consulting the ASTM G133-05 (2010) specifications, although the specifications were not strictly adhered to because of the limitations of test setup. Moreover, our intention is to see the effect of alternate wear and corrosion on the overall degradation of steel. The trend would be similar even if the standards were not strictly followed. Moreover, we have varied the loads to see the effect of load on the wear-corrosion as well corrosion-wear of two different types of steels. While the current results may not be directly comparable to those using the standard procedures, the authors propose that the reported trends would be similar. The steel samples were sized (20 mm × 20 mm × 5 mm) to fit in the groove of the sample holder of the wear testing machine. Wear testing was carried out in a linearly reciprocating ball-on-flat dry sliding wear tester (Reciprocatory Friction Monitor TR-287, DUCOM). The wear testing machine was capable of recording the tangential friction force along with normal load using the commercial Winducom 2006 software (DUCOM, India). All the samples were tested for three different load values (30, 40 and 50 N) with a stroke length of 10 mm for a total sliding distance was 50 m (2340 cycles). The frequency of oscillation was 5 Hz for all the test load values. Hardened steel ball of 8.3 mm diameter with hardness in the range of 800–900 HVN was used as the rubbing material on the coupon sized work piece made of the DPS and the MS steels. The DPS samples had hardness in a range of 240–250 HVN, and the MS samples had hardness in range of 130–135 HVN. The hardness of the balls was approximately 3–6 times than that of the work pieces. The geometry of the wear scar on the ball and flat specimen was observed in FEI Quanta scanning electron microscope using secondary electron mode. Electron dispersive spectroscopy (EDS) of the wear track was also performed to analyze the specific features, like white spots after corrosion. For wear volume calculation, the method used by Sharma et al. [30] was used. The wear volume in mm^3 was calculated using Eq. (1). This method involves measuring the wear scar dimensions and the steel ball worn out surface dimensions using a simple optical microscope.

$$V' = L\left[\left\{r^2 \sin^{-1}\left(\frac{w}{2r}\right) - \frac{w}{2}\left(r^2 - \frac{w^2}{4}\right)^{\frac{1}{2}}\right\} - \left\{r^2 \sin^{-1}\left(\frac{w'}{2r}\right) - \frac{w'}{2}\left(r^2 - \frac{w'^2}{4}\right)^{\frac{1}{2}}\right\}\right] + \frac{\pi}{3}\left[2r^2\left\{\left(r^2 - \frac{w'^2}{4}\right)^{\frac{1}{2}} - \left(r^2 - \frac{w^2}{4}\right)^{\frac{1}{2}}\right\} - \frac{w^2}{4}\left(r^2 - \frac{w^2}{4}\right)^{\frac{1}{2}} + \frac{w'^2}{4}\left(r^2 - \frac{w'^2}{4}\right)^{\frac{1}{2}}\right] \quad (1)$$

where w = width of the cylindrical section of the wear scar, w' = diameter of the wear scar on the ball, r = radius of the ball, L = stroke length, L and w can be measured directly from the wear

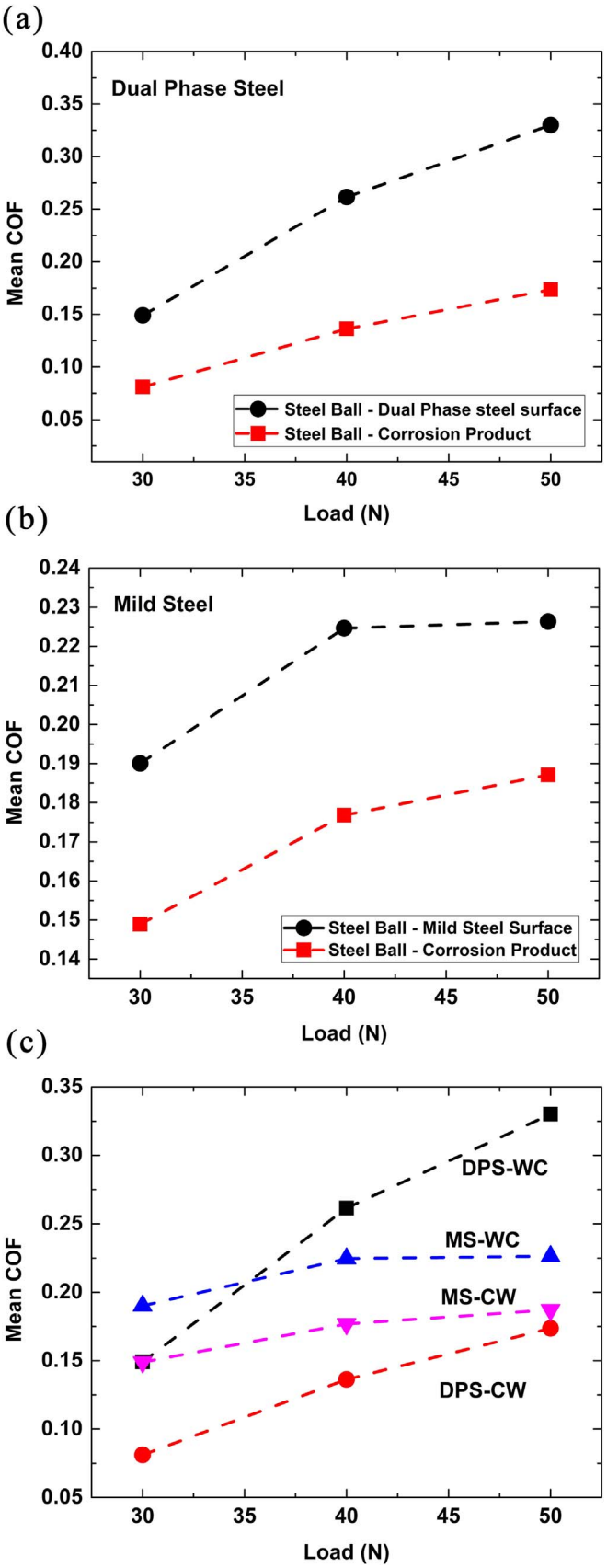

Fig. 5. Mean coefficient of friction (C.O.F) for the (a) DPS and (b) MS for WC and CW cases. (c) Comparison of the C.O.F for the DPS and MS.

scar cylindrical segment. The ball radius, r, is known to be (8.3/2=4.15 mm) and w' can be measured from the ball scar or alternatively from the following equations:

$$h = r - \left(r^2 - \frac{w^2}{4}\right)^{\frac{1}{2}} h' = r - \left(r^2 - \frac{w^2}{4}\right)^{\frac{1}{2}} \quad (2)$$

where h=depth of the wear scar, h'=depth of the cylindrical section which is not a part of the actual wear scar.

3. Results and discussions

3.1. Microstructure

The optical micrographs of the DPS and MS are shown in Fig. 2. The average grain size of the DPS is 5 μm with around 22% volume fraction of uniformly distributed martensite islands in ferrite matrix (Fig. 2(a)). The average grain size in the MS is around 15 μm with a matrix of equiaxed and uniformly distributed ferrite grains (Fig. 2(b)). On accounts of very low carbon content, the pearlite fraction is insignificant to be even visible in optical micrographs.

3.2. Wear volume and mean C.O.F

Fig. 3 shows the wear scars for the WC and the CW case of both the steels at normal loads 30 N, 40 N and 50 N. It has been observed that width of the wear scar increases with load in general. For all the CW case, it is very clear that the rust layer is flattened on in the wear track and rust layer tries to get accumulated on the edge of the wear track. The rust layer is ploughed off to the sides of wear track and the extent of ploughing increases with increasing normal load. This phenomenon has been observed for both the DPS (Fig. 3(a1–a3) and (b1–b3)) and the MS (Fig. 3(c1–c3) and (d1–d3)). The white spots visible on the rust layer are of the deposited NaCl residues from the immersion corrosion (EDS data not shown).

Fig. 4 shows the variation of wear volume as a function of normal loads for the DPS (Fig. 4(a)) and the MS (Fig. 4(b)). The wear volumes of the WC and CW cases are compared for both the steels in Fig. 4(c). It is to be mentioned that the wear volume in case of the WC cases has been measured before subjected to corrosion test. The wear volume increases with normal load. There is a considerable decrease in wear volumes for the samples for the CW case as compared to the samples of the WC case. This behavior has definitely been found to be material independent. Though the magnitude of wear volume is different, but the similar phenomenon has been observed for both the steels. It can be attributed that the presence of rust layer on the steels (CW case) has resulted in wear volume reduction by about 23–30% for the DPS and around 23–48% for the MS steel depending on the load in case of the CW. This trend suggests that the lubricating nature of the rust formed during immersion corrosion protects the steel surface against the abrading action of the steel ball. Wear volumes at all wear loads are shown in Table 2.

Comparative nature of wear volumes of the DPS and MS (Fig. 4(c)) show higher wear resistance of the DPS as compared to the MS. This trend could be attributed to the microstructures of the DPS and the MS. Martensite islands in ferrite matrix render higher surface hardness to the DPS as opposed to relatively soft ferrite matrix with insignificant pearlite fraction in the MS. Since the presence of pearlite is not visible in case of the MS, the sole presence of soft ferrite matrix would lead to further wear damage and substantial wear volumes. It is well known that as per the Arachard model [31,32] for sliding wear, total wear volume of debris is inversely proportional to hardness of the softest contacting surface. Additionally, smaller grain size

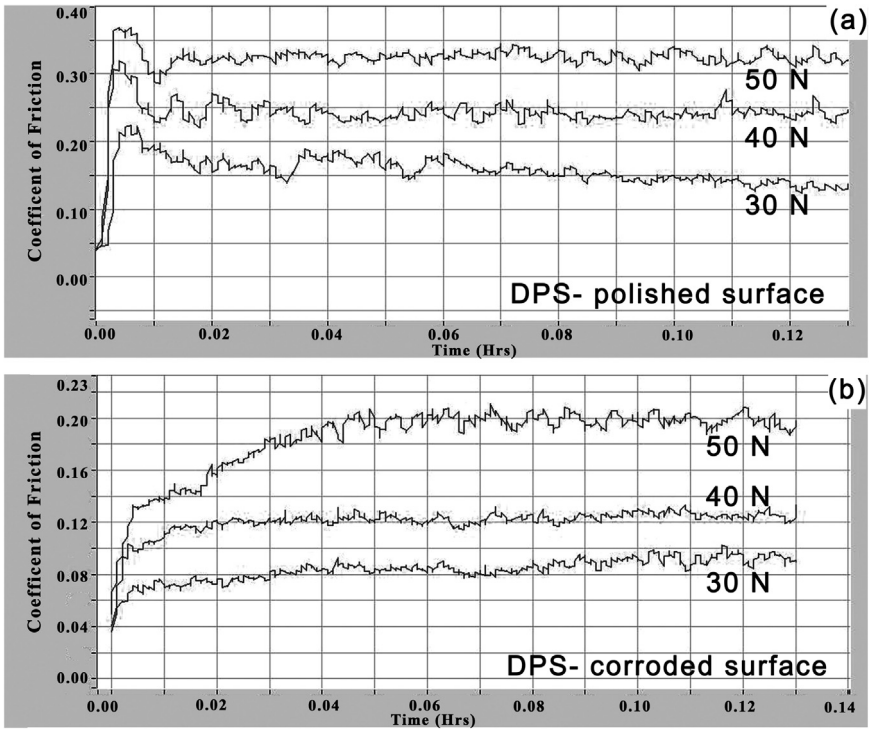

Fig. 6. Representative machine data for the mean coefficient of friction for the (a) DPS-WC and (b) DPS-CW.

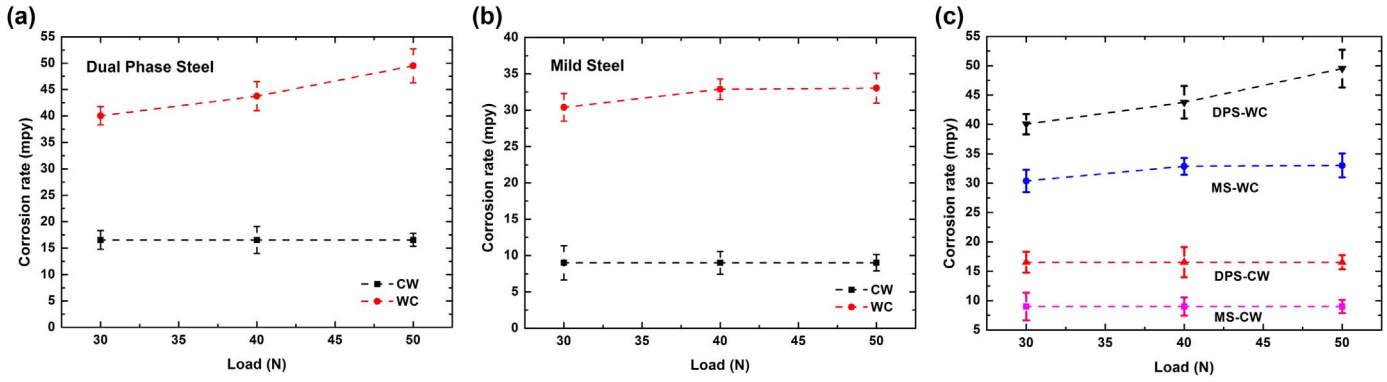

Fig. 7. Corrosion rates for the (a) DPS and (b) MS for WC and CW cases. (c) Comparison of corrosion rates for the DPS and MS.

of the DPS as compared to the MS imparts higher work hardening effect in the DPS. All these factors allow the DPS to possess a superior wear resistant, assuming the extent of lubrication provided by the rust is same. It is to be mentioned that our main objective is to see the relative effect of the WC and CW cases on two different steels. In addition, we present the effect of microstructures of the steels on the WC and CW cases.

Fig. 5 shows the variation of the mean coefficient of friction (COF) as a function of normal wear load for the DPS (Fig. 5(a)) and the MS (Fig. 5(b)). It is to be mentioned that the COF in the WC cases is measured just after wear test and before the sample is subjected to corrosion. This has been done just to avoid the effect of corrosion on the COF. It has been realized that the corrosion products provides lubricating action (explained later). Moreover, the wear test could not be carried out exactly on the earlier worn out zone after corrosion in case of the WC case since the worn out zone in the first go is also covered with corrosion products after corrosion. The COF of the WC and the CW cases are compared for each steel (Fig. 5(c)). It is clearly evident that the mean COF increases with normal load and this trend is independent of nature of steel (whether DPS or MS). Since normal load increases, the shear force between the abrading steel ball and the steel surface also increases. This leads to increase in the mean COF. It is interesting to note that the mean COF for the CW case is considerably lower than that in the WC case and this is common for both the steels. This trend supports to the lubricating action of the rust layer formed during initial immersion corrosion. This is also noted in case of the trend in wear volume for both the steels.

Owing to higher hardness, the DPS has a higher mean COF than the MS at all loads (Fig. 5(c)). It is worth noting that the trend of change in wear volume and mean COF go hand in hand for both the steel and for all the respective cases. The mean values of the COF are derived from the machine generated data as shown in representative Fig. 6, depicting the variation of COF for the DPS with time in cases of WC (Fig. 6(a)) and CW (Fig. 6(b)). The corresponding values of the mean COF at various normal wear loads are given in Table 2.

3.3. Corrosion rate and Corrosion product analysis

Fig. 7 shows the corrosion rates of the DPS (Fig. 7(a)) and the MS (Fig. 7(b)) as a function of normal wear loads for the WC and

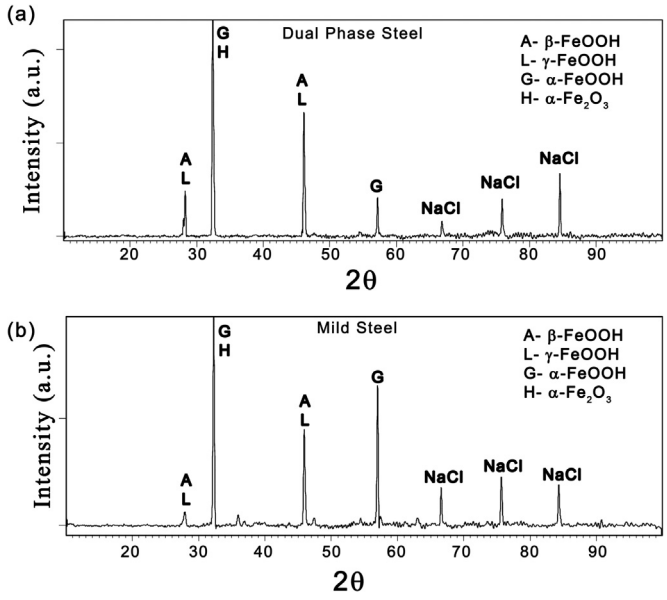

Fig. 8. X-ray diffraction patterns of the rust from the (a) DPS and (b) MS after corrosion only.

the CW cases. For the WC cases, it has been observed that the corrosion rate of the wear tested samples increases with increasing normal wear loads, and this trend is independent of steel type. This behavior could be justified on the basis of the Hertzian contact pressure [33] and effect of pre-deformation [34] stresses on corrosion behavior of steels. Table 2 shows the values of the Hertzian contact pressure corresponding to various normal wear loads. The Hertzian contact pressure increases linearly with normal load and is considerably higher in magnitude than the respective yield strengths of both the steels. These high values of the Hertzian contact pressures result in severe surface plastic deformation, which introduces high dislocation density and compressive stresses on the steel surface. High surface dislocation density leads to high rates of uniform corrosion [34], whereas high localized surface compressive stresses lead to localized corrosion attack. It is interesting to note that the compressive stresses are present in the wear track only. Hence, the dissolution rate will definitely be faster in the wear track as compared to the surrounding region, which corrodes as per the characteristics of as-received surface. This explains the increase in corrosion rate with the increase in normal wear loads, irrespective of steel types. In this aspect, it is worth mentioning that surface compressive stress helps in improving the stress corrosion resistance, by reducing the effect of tensile stress component, which actually is the reason for crack opening. However, in the case of wear, it actually increases the electrochemical activity of the surface with high compressive stress on the wear surface, leading to higher corrosion attack.

Since for the CW case immersion corrosion tests have been carried out before the wear tests, the corrosion rates are independent of wear loads. Fig. 7(c) shows corrosion rate comparison of the DPS and the MS for both the WC and CW cases, and it is noteworthy that the corrosion rate of the DPS is higher than the MS. This trend in corrosion rate could be reasonably justified on the basis of effect of microstructure on the corrosion rate of steel [35]. The smaller grain size of the DPS results in higher grain boundary area, and grain boundaries are potential sites for corrosion attack, thereby leading to high corrosion rates in the DPS as compared to the MS. Generally, higher carbon content in ferritic steel leads to higher corrosion susceptibility [35]. From Table 1, it is very clear that the DPS steel has higher carbon percentage than that of the MS steel. Hence, corrosion susceptibility of the DPS steel is higher than of the MS steel (Fig. 7(c)).

3.3.1. *X-ray diffraction*

Fig. 8 shows the X-ray diffraction patterns of the powder rust samples taken from the CW case of the DPS and MS samples. Diffraction patterns shows the presence of highly unstable iron hydroxide viz. lepidocrocite (γ-FeOOH) [36] along with traces of stable hydroxides like goethite (α-FeOOH) and akaganeite (β-FeOOH) [37]. Akaganeite phase is inevitably present, when steels are exposed to the atmospheres containing Cl^- ions or marine environments [36]. Goethite, which is one of the most stable phases of iron rust, evolves from lepidocrocite on oxidation in air. Diffraction patterns also show the presence of hematite (α-Fe_2O_3), and is one of the most stable iron oxides. NaCl, which precipitates from the immersion solution, is seen at higher diffraction angles ($2\theta^\circ = 67^\circ$, 76° & 85°). Identical rust phases have been found for both the DPS and MS rusts with a slightly higher proportion of goethite and a slightly lesser akaganeite and lepidocrocite content in the MS rust as indicated by the intensity ratio. The presence of phases obtained in X-ray diffraction technique has been again confirmed by the FTIR analysis of the powder rust.

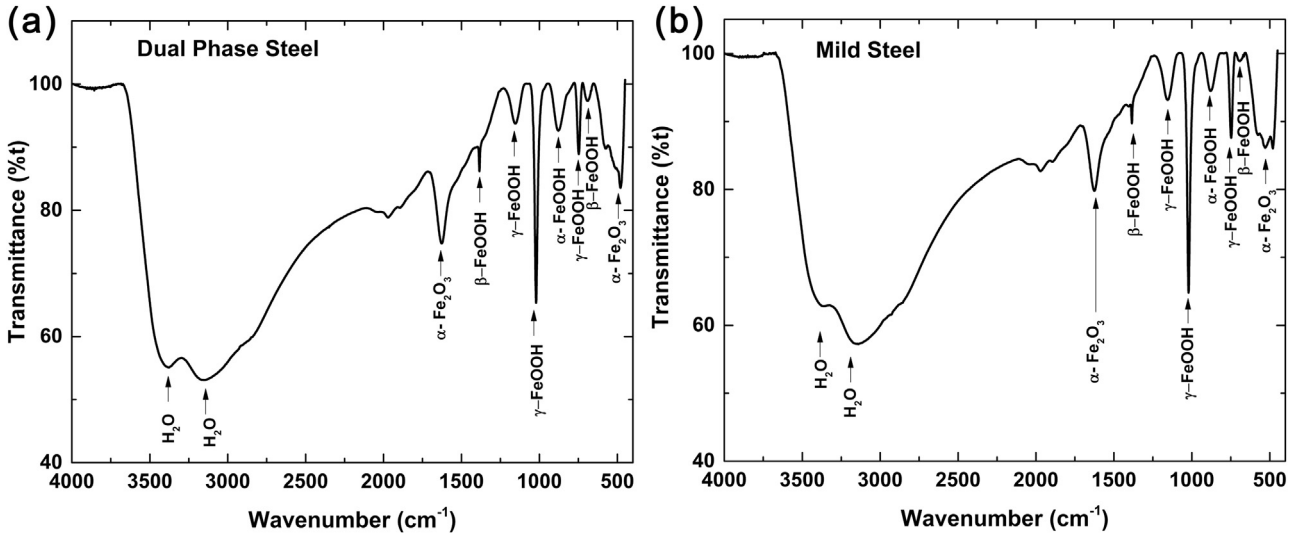

Fig. 9. FTIR spectrum of the rust obtained from the (a) DPS and (b) MS after corrosion only.

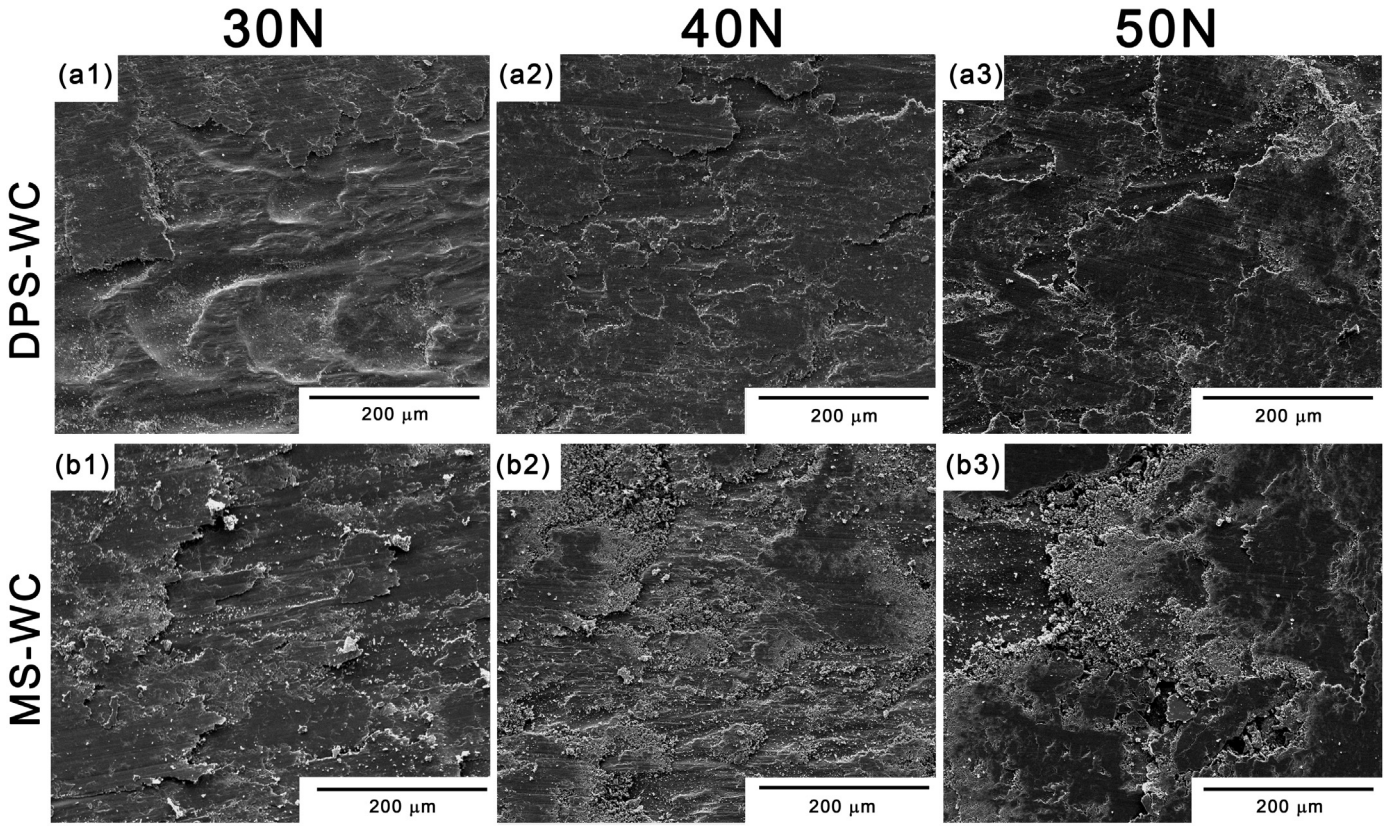

Fig. 10. Wear surface scar in the case of the WC at various loads for the (a1–a3) DPS and (b1–c3) MS.

3.3.2. FTIR analysis

Corrosion products can be characterized from the various known resonant vibration frequencies [38]. Fig. 9 shows the FTIR spectrum of the rusts obtained from the CW cases of the DPS (Fig. 9(a)) and the MS (Fig. 9(b)). The FTIR spectrum for both the steels clearly show that the corrosion product phases forming are unchanged suggesting that there is limited effect of steel's composition and microstructure on the rust constituents in the present conditions. FTIR spectrum further confirm the presence of various iron hydroxides, namely (1) Goethite (α-FeOOH), (2) Lepidocrocite (γ-FeOOH), (3) Akaganeite (β-FeOOH) and (4) hematite (α-Fe_2O_3), which were initially detected by X-ray diffraction technique. Misawa et al. [39] have pointed out that absorption band at higher wave number is due to O–H stretching, whereas the absorption band at lower wavelengths is due to Fe–O stretching vibration. Wave numbers from 3000 cm^{-1} to 3500 cm^{-1} can be associated with the H_2O within the bulk of iron (III) oxyhydroxides, and the wave numbers below 3000 cm^{-1} can be associated with various iron oxides and hydroxides.

It is important to mention that the nature of the rusts are almost similar in both the samples. It could be possible that the lubricating actions of the similar rusts in both the steels are also similar.

3.4. Wear surface analysis

3.4.1. WC case

Fig. 10 shows SEM micrographs of the wear scar surface for the WC cases of the DPS (Fig. 10(a1–a3)) and the MS (Fig. 10(b1–b3)) at various normal wear loads. Examination of wear scar surface gives an idea of change in severity of plastic deformation and the wear mechanisms. For the DPS samples, wear scar surface at 30 N shows shearing of the surface. However, no sign of de-lamination can be observed on the scar surface, which is indicative of very less/mild surface plastic deformation. In this case, the stresses due to sliding wear are just enough to shear the surface, but do not lead to surface de-lamination. At 40 N, the wear scar shows a mild to moderate surface delamination with metal film emerging out as brittle flakes (Fig. 10(a2)). On the contrary, at 50 N (Fig. 10(a3)), wear scar shows severe case of surface delamination with large amount of small metal fragments /chunks, which have resulted from spalling due to increased shear load.

The main cause of surface delamination is sub-surface nucleation and growth of fatigue cracks, which extends up to the surface levels and results in detachment of the metal fragment [40]. Additionally, the extent of adhesive wear increases with increasing normal loads. The metal chunks adhere and form a cold weld with the abrading steel ball, and during sliding reciprocatory motion they get delaminated from the base metal [4]. In subsequent stages of wear, metal chunks again stick back, weld to the base metal due to high normal, and shear forces, and the wear debris found in mid of the wear track manifests this. The presence of abrasive grooves is prominently observed with increasing normal loads.

For the MS-WC samples, the wear scar morphology shows a considerably higher surface delamination as compared to their respective DPS-WC counter parts at all normal loads. This is mainly due to low hardness of the MS as compared to the DPS. This also reduces the wear resistance of the MS. The fatigue loading due to reciprocating motion has a higher impact on nucleation of sub-surface fatigue cracks in the MS than in the DPS. This also indicates higher surface delamination in the MS (Fig 10 (b1–b3)). The extent of metal spalling increases with increasing normal load, resulting in large metal fragments and big metal patches delaminated from the steel surface (Fig. 10(b1–b3)). Abrasive grooves are observed in the MS right from the lower loads (till 30 N), whereas, this has not been observed in the case of the DPS at lower loads (~30 N). This can be attributed to the metal

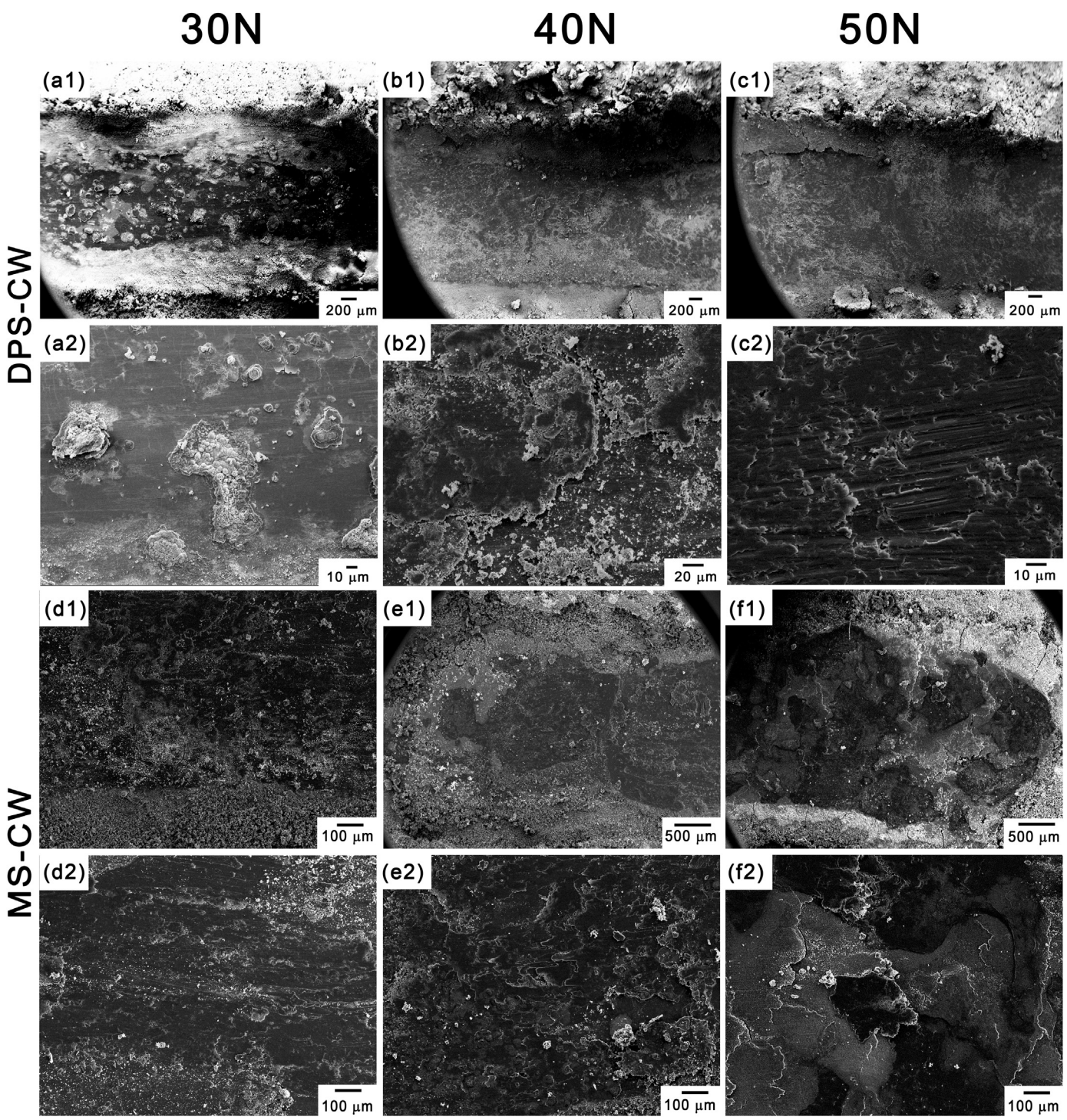

Fig. 11. Wear surface scar in the case of CW for the DPS samples at (a1,a2) 30 N, (b1,b2) 40 N and (c1,c2) 50 N, and for the MS samples at (d1,d2) 30 N, (e1,e2) 40 N and (f1,f2) 50 N.

fragments acting as hard particles between base metal and abrading steel ball. Additionally the presence of soft ferrite phase in the MS enhances the delamination as opposed to the presence of martensite phase in the DPS, preventing delamination in the DPS at lower loads.

3.4.2. CW case

Fig. 11 shows the wear scar surface in case of the CW at various normal loads for the DPS (Fig. 11(a1, a2, b1, b2, c1 and c2)) and the MS (Fig. 11(d1, d2, e1, e2, f1 and f2)). For both the steels and at all loads, the rust layer has been ploughed off to the sides of the wear track. However, the extent of the residual oxides on wear scar surface decreases with increasing normal loads. Ploughing of rust layer to the sides of the wear track results from the reciprocating sliding motion of the abrading steel ball along with high normal and shear loads. For the DPS at 30 N (Fig. 11(a1 and a2)), wear track shows the presence of fractured brittle oxide products on the scar surface. These oxides have formed during initial immersion tests. It is to be mentioned that the oxides are indicated with the appearance of secondary electron charging. The scar surface

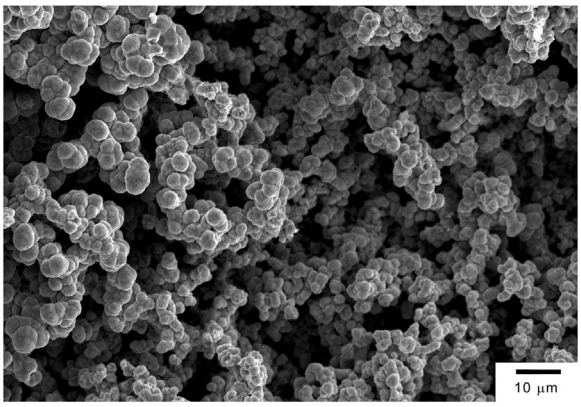

Fig. 12. Goethite morphology after corrosion only. This is common in both the steels.

morphology shows the wear to be intact and free of any cutting groves and severe deformation shear marks, which is indicative of the high lubricating nature of the rust layer, protecting the base metal from wear damage. However, at 30 N, the MS (Fig. 11(d1 and d2)) does not indicate any presence of residual rust products, which can be attributed to higher depth of penetration of abrading steel ball, due to lower hardness of the MS. Also at 30 N, the MS samples show the presence of abrasive grooves with no sign of metal delamination. This shows that the extent of protectiveness of the MS rust is less than that of the DPS. This behavior can be attributed to the rust layer thickness. Since the DPS samples have higher corrosion rates as compared to the MS steels (Fig. 7), the thickness of the rust layer is definitely going to be higher in case of DPS samples. Since the rust phases present in both the DPS and the MS are almost same, rust composition would have similar effect on the lubricating and protective nature of rust. Hence, higher thickness of the rust in case of the DPS gives better cushioning to reciprocating effect of the ball.

For the DPS samples, at 40 N (Fig. 11(b1 and b2)) and 50 N (Fig. 11(c1 and c2)), a large amount of metal fragments is observed on the wear track. This is attributed to the severe spalling of the base metal due to high shear loading. Deep surface abrasive grooves have been observed, which have resulted from the cutting and ploughing action [4,7] of in-situ high hardness rust particles. These rust particles give rise to three body abrasive wear mechanism. The third body in the abrasive wear is under rolling action, and this results in lower value of mean COF. However, it leads to formation of abrasive groove concurrently due to higher oxide hardness.

For the MS samples, at 40 N (Fig. 11(e1 and e2)) and 50 N (Fig. 11(f1 and f2)), the extent of the delamination and the metal spalling is higher than of the DPS. At highest normal wear load of 50 N, oxidative wear can be observed. This observation is made based on the secondary electron charging of the oxide particles. Since the residual rust from the immersion corrosion is not present on the wear track at high loads, the only possibility of the oxide formation is due to high temperature oxidative-wear. The nature of oxide film forming on the wear track is brittle in nature, which results in cracking on the sub-surface (Fig. 11(e2 and f2)). High oxygen content within the wear track from EDS study (data not shown) suggests this.

It is interesting to note that the extent of adhesive wear for the CW case is far less than that in the WC case. At initial stages of wear, the steel ball/base metal contact is cushioned by the rust layer. Additionally, the factor, which reduces adhesive wear, is the granular powder form of rust layer, preventing the cold welding between abrading steel ball and steel surface. Rust phase morphology plays a vital role, about mean COF, wear mechanism and wear volume. Goethite, which has a cotton ball structure (Fig. 12), and this gives higher rolling tendency and the COF reduces resulting lower wear volumes.

4. Conclusions

The purpose of this investigation of reciprocating sliding of two steels was to study the effects of sequential combinations of corrosion after wear WC) or wear after corrosion (CW). The steels were mild steel (MS) and dual-phase steel (DPS). The corrosive solution was 3.5 wt% NaCl). Based on comparative experiments, the following conclusions were obtained from this study:

(1) The wear volume of DPS in both situations (WC and CW) is lower than that for MS. This was proposed to result from differences in microstructure.
(2) In general, the wear volume of CW exposure is less than for WC exposure. This result is proposed to be a result of the rust that formed during the CW process. This behavior was independent of the type of steel or applied load.
(3) The corrosion rate of DPS exposed to WC is higher than for the MS. In addition, the corrosion rate of both steels increases when wear occurs first (WC). The latter is proposed to result from microstructural deformation during the early stages of wear.

Acknowledgement

The authors are grateful to Dr. S. Kundu of TATA Steel - Jamshedpur, Jharkhand, India for providing the dual phase steel to carry out this research.

References

[1] M.A. Moore, The relationship between the abrasive wear resistance, hardness and microstructure of ferritic materials, Wear 28 (1974) 59–68.
[2] N. Ojala, K. Valtonen, V. Heino, M. Kallio, J. Aaltonen, P. Siitonen, et al., Effects of composition and microstructure on the abrasive wear performance of quenched wear resistant steels $, Wear 317 (2014) 225–232.
[3] S.Q. Wang, L. Wang, Y.T. Zhao, Y. Sun, Z.R. Yang, Mild-to-severe wear transition and transition region of oxidative wear in steels, Wear 306 (2013) 311–320.
[4] K.G. Budinski, Friction, Wear, and Erosion Atlas, 1998.
[5] X. Xu, S. Van Der Zwaag, W. Xu, The effect of ferrite – martensite morphology on the scratch and abrasive wear behaviour of a dual phase construction steel, Wear 349 (2016) 148–157.
[6] S. Sharma, S. Sangal, K. Mondal, Wear behavior of newly developed bainitic wheel steels, J. Mater. Eng. Perform. 24 (2014) 999–1010.
[7] A. Fischer, K. Bobzin, Friction, Wear and Wear Protection, Wiley-VCH GmbH & Co. KGaA, 2009.
[8] A. Sharma, A. Kumar, R. Tyagi, Erosive wear analysis of medium carbon dual phase steel under dry ambient condition, Wear 335 (2015) 91–98.
[9] A. Bayram, A. Uguz, Effect of microstructure on wear behaviour of dual phase steel, Thin Solid Films 304 (1997) 61–64.
[10] X. Xu, S. Van Der Zwaag, W. Xu, The effect of martensite volume fraction on the scratch and abrasion resistance of a ferrite – martensite dual phase steel, Wear 349 (2016) 80–88.
[11] E. Ahmad, T. Manzoor, M.M.A. Ziai, N. Hussain, Effect of martensite morphology on tensile deformation of dual-phase steel, J. Mater. Eng. Perform. 21 (2012) 382–387.
[12] H. Goto, Y. Amamoto, Improvement of wear resistance for carbon steel under unlubricated sliding and variable loading conditions, Wear 270 (2011) 725–736.
[13] P. Andersson, B. Hemming, Determination of wear volumes by chromatic confocal measurements during twin-disc tests with cast iron and steel, Wear 338–339 (2015) 95–104.
[14] a Trausmuth, M. Rodriguez ripoll, G. Zehethofer, T. Vogl, E. Badisch, Impact of corrosion on sliding wear properties of low-alloyed carbon steel, Wear (2015) 338–347.
[15] J.L. Sullivan, S.S. Athwal, The role of oxidation in the wear of alloys, Tribology Int. 16 (1983) 123–131 (n.d.).
[16] J.F. Archard, W. Hirst, The wear of metals under unlubricated conditions, Proc.

R. Soc. A 236 (1956) 397–410.
[17] F.H. Stott, M.P. Jordan, The effects of load and substrate hardness on the development and maintenance of wear-protective layers during sliding at elevated temperatures, Wear 250 (2001) 391–400.
[18] H. Goto, Y. Amamoto, Effect of varying load on wear resistance of carbon steel under unlubricated conditions, Wear 254 (2003) 1256–1266.
[19] A. Islam, T. Alam, Z.N. Farhat, A. Mohamed, A. Alfantazi, Effect of microstructure on the erosion behavior of carbon steel, Wear. 332- 333 (2015) 1080–1089.
[20] K.D. Ralston, N. Birbilis, Effect of grain size on corrosion, Corrosion 66 (2010) 1–4.
[21] P.P. Sarkar, P. Kumar, M.K. Manna, P.C. Chakraborti, Microstructural influence on the electrochemical corrosion behaviour of dual-phase steels in 3.5% NaCl solution, 2005.
[22] L.R. Bhagavathi, G.P. Chaudhari, S.K. Nath, Mechanical and corrosion behavior of plain low carbon dual-phase steels, 2011.
[23] J. Alcántara, B. Chico, J. Simancas, I. Díaz, D. de la Fuente, M. Morcillo, An attempt to classify the morphologies presented by different rust phases formed during the exposure of carbon steel to marine atmospheres, Mater. Charact. 118 (2016) 65–78.
[24] R.J.K. Wood, S.P. Hutton, The synergistic effect of erosion and corrosion: trends in published results, 1990.
[25] R. Malka, S. Nešić, D.A. Gulino, Erosion–corrosion and synergistic effects in disturbed liquid-particle flow, Wear 262 (2007) 791–799.
[26] R.J.K. Wood, Erosion–corrosion interactions and their effect on marine and offshore materials, Wear 261 (2006) 1012–1023.
[27] M.M. Stack, G.H. Abdulrahman, Mapping erosion-corrosion of carbon steel in oil exploration conditions: some new approaches to characterizing mechanisms and synergies, Tribiology Int. 43 (2010) 1268–1277.
[28] E. Mahdi, A. Rauf, S. Ghani, A. El-Noamany, A. Pakari, Erosion-corrosion behavior and failure analysis of offshore steel tubular joint, Int. J. Electrochem. Sci. 8 (2013) 7187–7210.
[29] M. Stack, J. James, Q. Lu, Erosion–corrosion of chromium steel in a rotating cylinder electrode system: some comments on particle size effects, Wear 256 (2004) 557–564.
[30] S. Sharma, S. Sangal, K. Mondal, On the optical microscopic method for the determination of ball-on-flat surface linearly reciprocating sliding wear volume, Wear 300 (2013) 82–89.
[31] J.F. Archard, W. Hirst, The Wear of Metals under Unlubricated Conditions, Proc. R. Soc. (1956) 397–410.
[32] J.F. Archard, J.F.A. Charj, Contact and rubbing of flat surfaces, J. Appl. Phys. 24 (1953), 32003–23502.
[33] N.P. Suh, H.C. Sin, The genesis of friction, Wear 69 (1981) 91–114.
[34] S.A. Al-duheisat, A.S. El-amoush, Effect of deformation conditions on the corrosion behavior of the low alloy structural steel girders, Mater. Des. 89 (2016) 342–347.
[35] J. Guo, S. Yang, C. Shang, Y. Wang, X. He, Influence of carbon content and microstructure on corrosion behaviour of low alloy steels in a Cl-containing environment, Corros. Sci. 51 (2009) 242–251.
[36] M. Morcillo, D. De La Fuente, I. Díaz, H. Cano, Atmospheric corrosion of mild steel; Corrosión atmosférica del acero suave, Rev. Metal. 47 (2011) 426–444.
[37] Y. Zhao, H. Ren, H. Dai, W. Jin, Composition and expansion coefficient of rust based on X-ray diffraction and thermal analysis, Corros. Sci. 53 (2011) 1646–1658.
[38] T. Misawa, K. Hashimoto, S. Shimodaira, The mechanism of formation of iron oxide and oxyhydroxides in aqueous solutions at room temperature, Corros. Sci. 14 (1974) 131–149.
[39] T. Misawa, K. Asami, K. Hashimoto, S. Shimodaira, The mechanism of atmospheric rusting and the protective amorphous rust on low alloy steel, Corros. Sci. 14 (1974) 279–289.
[40] N.P. Suh, An overview of the delamination theory of wear, Wear 44 (1977) 1–16.